journal

J. Am. Ceram. Soc., **84** [10] 2377–84 (2001)

Effect of Flaw State on the Strength of Brittle Coatings on Soft Substrates

Hae-Won Kim,[†] Yan Deng,[‡] Pedro Miranda,[§] Antonia Pajares,[¶] Do Kyung Kim,[*,††] Hyoun-Ee Kim,[*,‡‡] and Brian R. Lawn[**]

Materials Science and Engineering Laboratory, National Institute of Standards and Technology (NIST), Gaithersburg, Maryland 20899

A study is made of the role of flaw state on the strength properties of brittle ceramic coating layers bonded to soft polycarbonate substrates. We introduce Vickers radial cracks at prescribed loads into the coating undersurfaces prior to bonding to control the sizes and locations of the starting flaws. A spherical indenter is then loaded on the top bilayer surfaces, directly above the Vickers indentation sites, subjecting the radial cracks to flexural tensile stress. Radial crack responses are monitored *in situ*, using a camera located below the transparent substrate. Critical loads to cause radial crack instability, and ensuing growth of the arrested cracks, are recorded. Conventional biaxial flexure tests on corresponding monolith coating materials provide a baseline for data comparison. Relative to the monolith flexure specimens, the bilayers show higher strengths, the more so the larger the flaw, indicating enhanced flaw tolerance. A simple fracture mechanics analysis of the radial crack evolution in the concentrated-load field, with due account for distribution of flexural tensile stresses at the coating undersurface, is unable to account completely for the enhanced bilayer strengths for the larger Vickers flaws. It is hypothesized that the epoxy used to bond the bilayer components enters the cracks, causing crack-wall adherence and providing an increased resistance to radial crack instability. The fracture mechanics are nevertheless able to account for the arrest and subsequent stable extension of the radial cracks beyond the critical loads once this extraneous adherence has been overcome.

I. Introduction

BRITTLE coatings on soft substrates are prone to failure in concentrated surface loading by transverse "radial" cracking from far-field flexure tensile stresses at the lower coating surfaces.[1–11] Radial cracks initiate at a critical load, propagate upward and outward in an elongate geometry, arresting within the lower half of the coating and at some relatively large lateral distance from the loading axis. Further loading continues to extend the cracks, in a stable manner, maintaining the quasi-elliptical fracture geometry. Because the critical loads can be low, especially in thinner coatings, and can extend over long subsurface distances, radial cracks are highly deleterious. More conventional Hertzian "cone" cracks can also initiate from the upper, near-contact surface,[9] but since these initiate first only in the thickest coatings, and are less likely to lead to premature failures, they will not be considered further here.

Surface flaw state is an important factor in radial crack initiation. For instance, pre-abrading the lower surfaces of polished glass layers with SiC grit before joining to the substrate lowers the ensuing critical load by an order of magnitude and greatly reduces the scatter.[9] The issue of flaw state is especially important in the context of coating lifetime. A coating may begin with relatively flaw-free undersurfaces, but may incur damage at those surfaces during final joining to the substrate or during in-service operation. Examples are all-ceramic dental crowns, which are often pre-abraded at their inner surfaces to remove any excess material and to provide good cement adhesion to the tooth,[8] and thermal barrier coatings, which tend to develop interfacial flaws from oxidation processes.[12] Knowledge of the evolution of such flaws in subsequent tensile loading can be an important element in the coating design.

In the present study, we use controlled flaws to investigate the influence of flaw size on the critical load for subsurface radial cracking. For this purpose, we test model bilayers of ceramic slabs (coatings) bonded to soft polycarbonate underlayers (substrates) with epoxy adhesive. The bulk of testing is done on glass coating layers, but other ceramics are also tested to demonstrate generality. Polycarbonate is chosen for its transparency, enabling *in situ* observation of crack evolution in the coating lower surface from beneath the indenter.[9,10] The controlled flaws are introduced into the ceramic undersurfaces using a Vickers indenter at prescribed loads prior to bonding to the substrate. The bilayers are then loaded at their top surfaces with a spherical indenter, aligning the load axis with the Vickers flaw center, and the development of the ensuing radial cracks is monitored. Fracture mechanics analysis of the coating flexure beneath the sphere contact, taking into account the distribution of tensile stresses at the lower coating surface, enables calculation of effective strengths of the coatings (from the critical loads) and crack pop-in lengths. We show that the calculated bilayer strengths tend to higher values than those for comparative biaxial strength specimens of corresponding ceramic monoliths, especially for larger Vickers flaws, indicating some extraneous restraining role of the epoxy adhesive on crack instability.

II. Experimental Procedure

Soda-lime glass slides 75 mm × 25 mm × 1 mm were chosen as our primary brittle coating material for fabrication of test

J. E. Ritter Jr.—contributing editor

Manuscript No. 188177. Received October 27, 2000; approved April 20, 2001.

Supported by internal funding from the U.S. National Institute of Standards and Technology, and study leave grants from the Universidad de Extremadura, Spain and the Seoul National University, Korea. Partial support was also provided by the U.S. National Institute of Dental Research.

*Member, American Ceramic Society.

**Fellow, American Ceramic Society.

[†]Currently a Ph.D. student at School of Materials Science and Engineering, Seoul National University, Seoul 151-742, Korea.

[‡]Currently a Ph.D. student at Dept. of Materials and Nuclear Engineering, University of Maryland, College Park, MD 20742.

[§]Currently a Ph.D. student at Dept. Electrónica e Ingenierìa Electromecánica, Escuela de Ingenierías Industriales, Universidad de Extremadura, 06071 Badajoz, Spain.

[¶]Currently with Dept. de Física, Facultad de Ciencias, Universidad de Extremadura, 06071 Badajoz, Spain.

[††]Currently at Dept. of Materials Science and Engineering, Korea Advanced Institute of Science and Technology, Yusong, Taejon 305-701, Korea.

[‡‡]Currently at School of Materials Science and Engineering, Seoul National University, Seoul 151-742, Korea.

bilayers. Additional bilayers were fabricated using fine-grain ceramics from earlier studies:[11,13] porcelain[§§] (Vita Mark II®, Vita Zahnfabrik, Bad Sackingen, Germany), alumina (AD999, Coors Ceramics, Golden, CO), and zirconia (Y-TZP, Norton–St. Gobain, Raleigh, NC). The ceramics were in the form of plates with a minimum lateral surface dimension 15 mm and were polished to thicknesses d = 0.4–1 mm. Transparent polycarbonate plastic slabs 12.5 mm thick (AIN Plastics, Norfolk, VA) were used for the substrates.[9] Properties of these materials are listed in Table I.

Bilayers were prepared as in Fig. 1(a). Vickers indents were first made on the lower surfaces of each ceramic layer at loads Q = 0.1–300 N, introducing radial cracks of surface dimension c. A minimum of five indents, depending on the coating thickness and indentation load, could be placed on any one surface without neighbor–neighbor interactions. The coatings were then joined to the polycarbonate sublayers with a transparent epoxy (Harcos Chemicals, Bellesville, NJ) under light pressure for 24 h with a resultant adhesive thickness of 10–15 μm. Since the elastic properties of the adhesive are similar to those of the polycarbonate base,[9,14] the finished laminates are near-ideal ceramic/substrate bilayers.

The top surfaces of the bilayers were then loaded with a WC sphere (Fig. 1) of radius r = 3.96 mm on an Instron testing machine (Model 1122, Instron, Canton, MA), using an optical zoom system (Optem, Santa Clara, CA) with a video camcorder (Canon XL1, Canon, Lake Success, NY) to view the lower coating surface *in situ* through the polycarbonate base.[9] After a given Vickers indent was centered along the Instron load axis, the sphere was loaded and the ensuing radial crack evolution recorded. The critical loads P_R for unstable crack extension and subsequent stable extension of the popped-in cracks at $P > P_R$ were thus measured. These tests were run in air at a fixed Instron crosshead speed, adjusted to give fracture in ~10 s.

Comparative biaxial flexure tests were run on monolithic glass disks radius of 11.5 mm, cut from the same microscope slides, and containing similar Vickers indents on their undersurfaces, using a conventional half-sphere with flat (a = 3.18 mm) on three-ball support (b = 7.50 mm)[15] (Fig. 1(b)). Again, the tests were carried out in air and the Instron cross-head speed was adjusted to attain critical loads for radial crack instability in approximately the same time (~10 s) as the bilayer specimens. In a select few cases the Vickers indentations were covered with a thin layer of epoxy adhesive prior to testing.

III. Fracture Mechanics

(1) Stress Fields

In this section we present a finite element analysis of "hoop" tensile stresses acting on the prospective radial crack plane through the load axis and perpendicular to the coating surface (Fig. 1(a)). The algorithm, described in detail elsewhere,[14] models a WC indenter of radius r = 3.96 mm in frictionless axisymmetric contact with the top surface of a coating of prescribed thickness d and prescribed modulus E_c (Table I) bonded to a substrate of fixed thickness 12.5 mm and modulus E_s = 2.35 GPa by an infinitesimally thin, infinitely strong interlayer. The sphere is loaded to peak value in 70 increments, and the stresses evaluated at chosen intervals. It is assumed that the materials deform elastically everywhere.[9]

Contours of the tensile hoop stresses on the radial crack plane for a glass coating of thickness d = 1 mm on a polycarbonate substrate are shown in Fig. 2, at loads marked. Black areas indicate regions of compressive stress, graded light areas indicate tensile stresses, in increments of 10 MPa. The stress gradient within the tensile region is pronounced, diminishing monotonically in both the R- and z-directions. Note that whereas the number of contours scales with load, the shape of the contours remains relatively invariant, implying geometrical similarity in the plate flexure beneath the contact, governed by coating thickness d. The contours bear a strong resemblance to the quasi-elliptical radial crack profile,[9] indicating a pennylike characteristic in the crack pattern.

Table I. Mechanical Properties for Constituent Layer and Indenter Materials[†]

Material	Young's modulus, E[‡] (GPa)	Poisson's ratio	Toughness T[§] (MPa·m$^{1/2}$)
Soda-lime glass	70	0.22	0.67
Porcelain (Mark II)	68	0.20	0.92
Alumina (AD999)	390	0.22	3.1
Zirconia (Y-TZP)	205	0.23	5.4
Polycarbonate	2.3	0.35	
Tungsten carbide	614	0.22	

[†]Data from Rhee *et al.*[13] [‡]Uncertainties in E estimated at <5%. [§]Uncertainties in T estimated at <20%.

To quantify this characteristic, write the radial distribution of hoop stress at the coating bottom surface as

$$\sigma(R_*) = \sigma_0 F(R_*) \tag{1}$$

with $F(R_*)$ a function of $R_* = R/d$ and σ_0 a maximum value at the crack center ($R_* = 0$) given by

$$\sigma_0 = \frac{P}{Bd^2} \log\left(\frac{CE_c}{E_s}\right) \tag{2}$$

with B and C dimensionless coefficients.[16] The function $F(R_*)$ is plotted in Fig. 3 as the solid curves, making the adjustments B = 1.35 and C = 1 to provide a best fit to Eq. (2). The function $F(R_*)$ depends in a minor way on the modulus mismatch between coating and substrate materials, but is effectively invariant for loads and thicknesses in the calculation ranges (P = 3–300 N and d = 0.1–10 mm) for any given coating/substrate combination. (These parameter evaluations are considered more accurate than those previously made by fitting Eq. (2) to limited experimental data for glass/polycarbonate substrates.[16]) Again, these results confirm a certain geometrical similarity in the coating stress field.

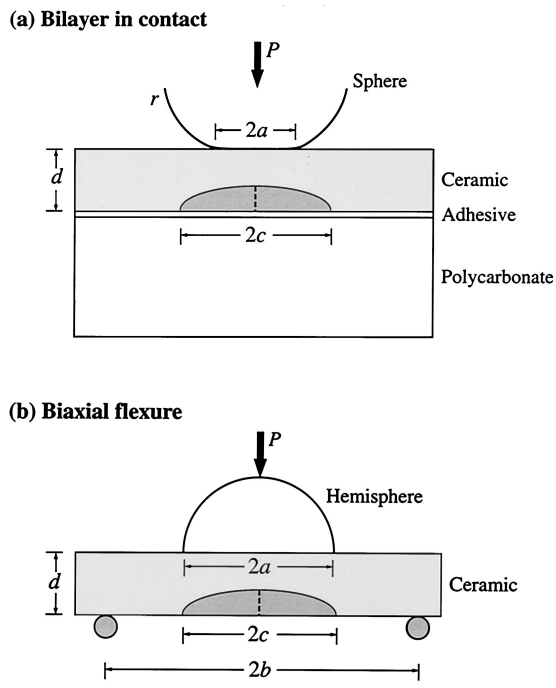

Fig. 1. Schematic of test configurations: (a) bilayer ceramic/polycarbonate (coating/substrate) specimen joined by epoxy adhesive, with Vickers preindentation radial flaw at ceramic undersurface; (b) comparative monolithic ceramic biaxial flexure specimen (flat on three-ball support).

[§§]Information on product names and suppliers in this paper does not imply endorsement by NIST.

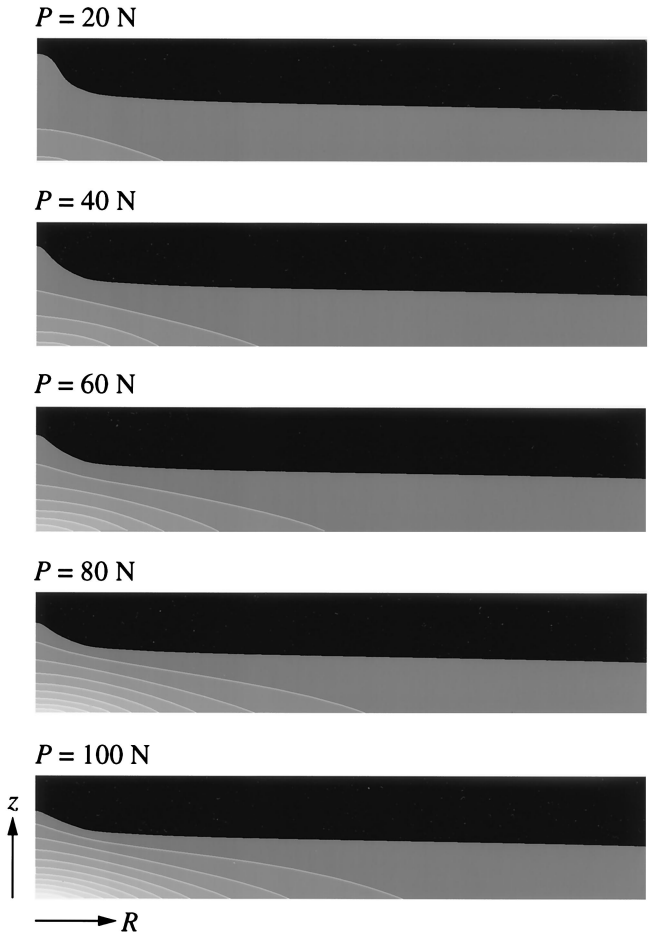

Fig. 2. FEM-generated contours of hoop stress in glass coating on polycarbonate substrate (not shown) at increasing contact loads indicated. Plots for glass thickness $d = 1$ mm. Each contour band represents a stress increase of 10 MPa, black region indicates compressive zone. Increasing load increases intensity of stress within tensile zone, but does not substantially alter shape of contours.

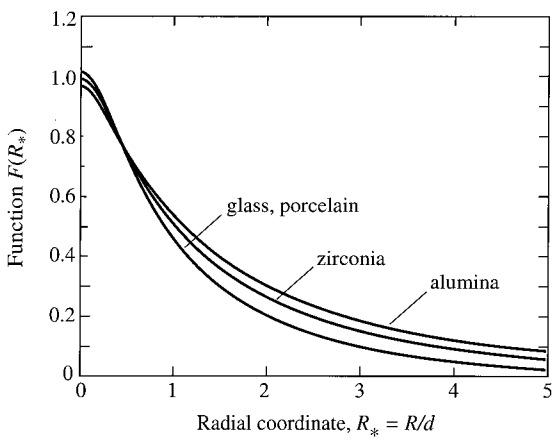

Fig. 3. Functions $F(R_*)$ in Eq. (1) for contact-induced tensile stresses on radial crack plane in bilayer ceramic coatings. Different coating materials (Table I) produce only slight variations in $F(R_*)$; variations for different sphere contact loads P and coating thicknesses d are indistinguishable on this plot.

It may be noted that Eq. (2) has the same functional form in relation to P and d:

$$\sigma_0 = \frac{P}{d^2} f\left(\frac{b}{a}\right) \tag{3}$$

for plates in biaxial flexure,[15] with σ_0 now independent of R_* and $f(b/a) = (3/16\pi)\{(1 + \nu)[2 \ln (b/a) + 1] + (1 - \nu)(2b^2 - a^2)/2R^2\}$ in the region $a \gg d$, confirming a dominant flexural component in the stress field for thin coatings on soft substrates.[7,9]

(2) Strength

The radial crack at the lower coating surface is subject to superposed driving forces from the residual stress field associated with the preceding Vickers load Q and the tensile field associated with the sphere contact at load P (Fig. 2). This becomes a complex fracture problem once the crack size c approaches the coating dimension d, as is inevitably the case after pop-in occurs at critical load $P = P_R$ (and perhaps even before, at sufficiently large Q), owing to a change in coating compliance. Neglecting this effect and any changes in crack shape with progressive extension, we may write an approximate stress-intensity factor in the generic form[17–19]

$$K = K_P + K_Q = \psi \sigma_0 c^{1/2} I(c_*) + \frac{\chi Q}{c^{3/2}} \tag{4}$$

with $c_* = c/d$, ψ a dimensionless crack geometry coefficient, and χ an elastic–plastic indentation coefficient. The integral quantity $I(c_*)$ allows for the diminishing radial stress field in Eq. (1):

$$I(c_*) = \int_0^{c_*} \frac{R_* F(R_*)}{c_*(c_*^2 - R_*^2)^{1/2}} \, dR_* \tag{5}$$

appropriate to pennylike cracks.[20] At equilibrium $K = T$, with T $(= K_{IC})$ the coating toughness (assumed single-valued), Eq. (4) may be solved for $\sigma_0(c)$:

$$\sigma_0(c) = \frac{T - \chi Q/c^{3/2}}{\psi c^{1/2} I(c_*)} \tag{6}$$

The "strength" $\sigma_0 = \sigma_F$ corresponding to the critical load $P = P_R$ for radial crack pop-in is then defined by the instability condition $d\sigma_0/dc > 0$.[20] Note the limiting case of large popped-in cracks, $c \gg (\chi Q/T)^{2/3}$:

$$\sigma_0(c) = \frac{T}{\psi c^{1/2} I(c_*)} \tag{7}$$

In the limit of $\sigma = \sigma_0 =$ constant independent of R_*, so that $F(R_*) = 1$ in Eq. (1) and $I(c_*) = 1$ in Eq. (5), Eq. (6) may be used to determine the familiar indentation–strength relation for monolithic ceramic plates in biaxial flexure. Imposing an instability condition $\sigma_0 = \sigma_F$ at $d\sigma(c)/dc > 0$ yields

$$\sigma_F = \frac{3}{4\psi}\left(\frac{T^4}{4\chi Q}\right)^{1/3} \tag{8}$$

with conventional $Q^{-1/3}$ load dependence.[18,21]

IV. Results

Generally, all materials showed well-developed Vickers radial crack patterns over the load range covered ($Q = 0.1$–300 N), with the following minor exceptions: a tendency to lateral crack chipping at higher loads ($Q > 50$ N) in the porcelain and to some extent in the glass,[22] and indication of constrained development (i.e., radial arm lengths less than twice the impression diagonals) at lower loads ($Q < 10$ N) in the zirconia.[23,24]

(1) Glass/Polycarbonate Bilayers

Figures 4 and 5 show radial crack sequences with increasing contacting sphere load P in glass/polycarbonate bilayers, at two Vickers indentation loads Q. The contact area between sphere and upper glass surface is evident in the micrographs as the expanding central circular shadow. In the first case, $Q = 30$ N, the cracks remain stationary as the load P is initially applied (Fig. 4(a)), then

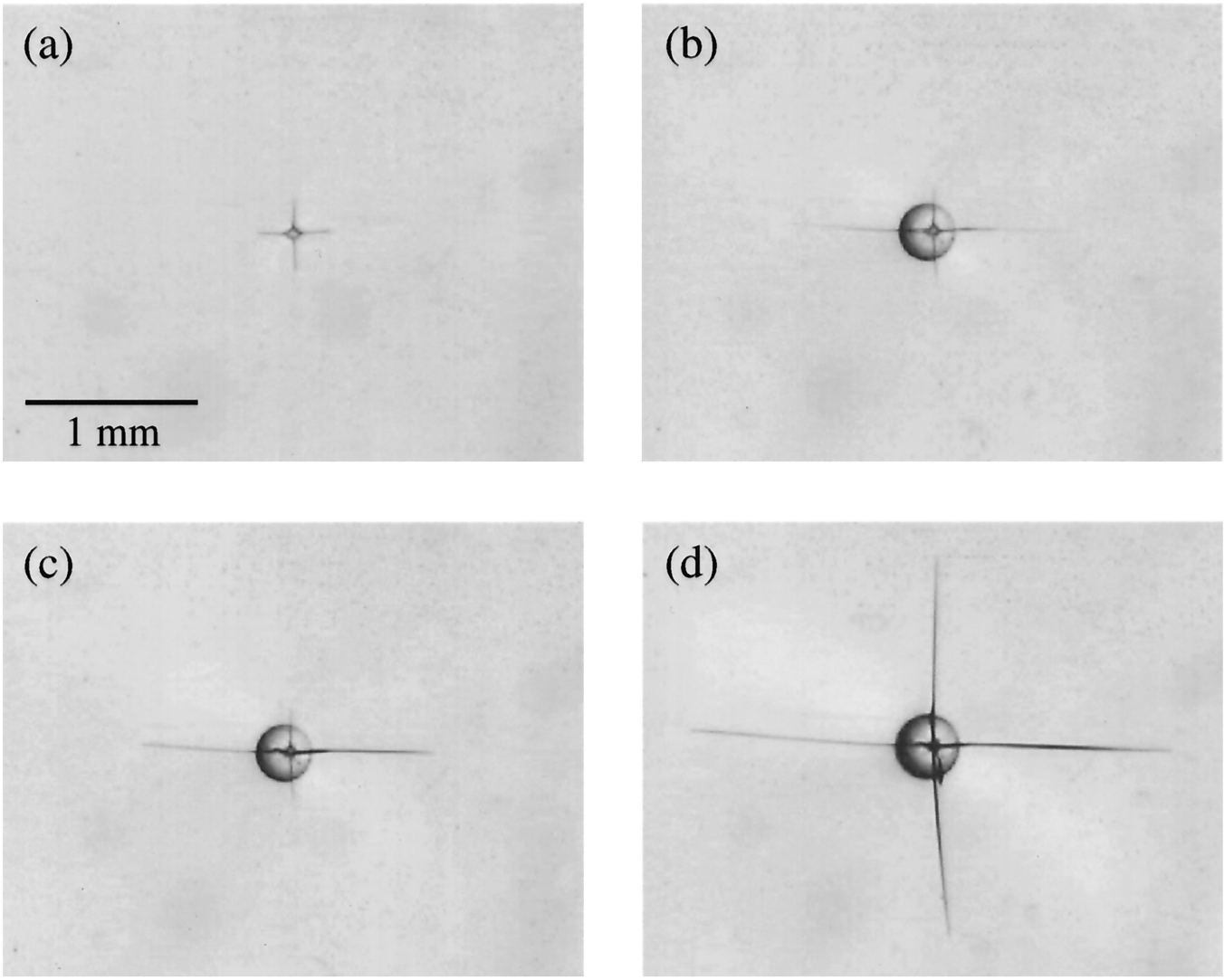

Fig. 4. Micrographs showing *in situ* radial crack growth evolution in glass/polycarbonate bilayers for Vickers load $Q = 30$ N, at the glass undersurface in glass/polycarbonate bilayer; sphere loads P (a) 0, (b) 68 N, (c) 70 N, and (d) 88 N. Showing initial radial crack, subsequent extension along first stable branch, pop-in, and continued stable extension.

begin to extend stably (Fig. 4(b)) until a distinct pop-in occurs at critical load $P_R = 70$ N (Fig. 4(c)), followed by further stable extension at $P > P_R$ (Fig. 4(d)). In the second case, $Q = 100$ N, the response is quite different: the initial crack remains stationary as P is applied (Figs. 5(a) and (b)) up to the point of instability, at which point an entirely new radial crack system initiates abruptly from the indentation zone (Fig. 5(c)) and, after arrest, extends stably (Fig. 5(d)) as in the previous case—in this example the initial crack never grows at all. The first kind of behavior was invariably observed at low load Q, with increasing incidence of the second kind of behavior at high Q. It is as if the epoxy somehow restrains the opening of the original crack walls at the larger indentations. Comparative observations on as-indented monolithic glass biaxial flexure specimens showed the usual precursor stable radial crack growth to instability,[18] with no subsequent arrest and second-stage stable branch and no secondary crack initiations.

In selected glass/polycarbonate bilayers the loading was stopped during the stable growth stages to observe the radial cracks more closely. In such cases the cracks continued to grow slowly at constant load, indicating that environmental moisture still has access to the subsurface cracks through the polymeric substrate[25] and that our assumption of crack equilibrium is, at best, a first approximation.

Figure 6 plots data for bilayer stress σ_0 as a function of measured crack size c from tests on glass/polycarbonate bilayers (filled symbols), with σ_0 evaluated from the applied contact load P using Eq. (2). Included in Fig. 6 are comparative $\sigma_0(c)$ data from monolith glass flexure tests (unfilled symbols), with σ_0 evaluated from Eq. (3). The data represent four Vickers loads Q, for several radial cracks at each load. For the bilayers, the data quantify the essential crack growth characteristics observed in the micrographs: an initial stationary phase, followed by stable growth to instability (dashed horizontal line), and then arrest and a second stage of stable growth. Again, pop-in is most pronounced at low Q. At high Q, either the original radial cracks grow stably through their entire evolution, i.e., without pop-in, or entirely new ones are abruptly initiated. For the monolith flexure specimens, the data confirm a precursor stage of stable growth, followed by unconditional failure at instability.

Figure 7 plots radial crack instability stress σ_F (corresponding to critical load $P = P_R$), or "strength," as a function of Vickers indentation load Q for glass/polycarbonate bilayers (circles), along with comparative data from monolithic glass biaxial flexure specimens (triangles). Data are means and standard deviations (minimum of five indentations). Note the striking tendency for the bilayer strength data to plateau out well above the monolith flexure data at higher Q. Filled symbols indicate failures from indentation sites, unfilled symbols from "natural" flaw sites on the as-polished surfaces. The open box at the left axis represents the strength of specimens without indentations—the Vickers radial cracks thus constitute dominant flaws in the glass surfaces at loads $Q > 0.1$ N.

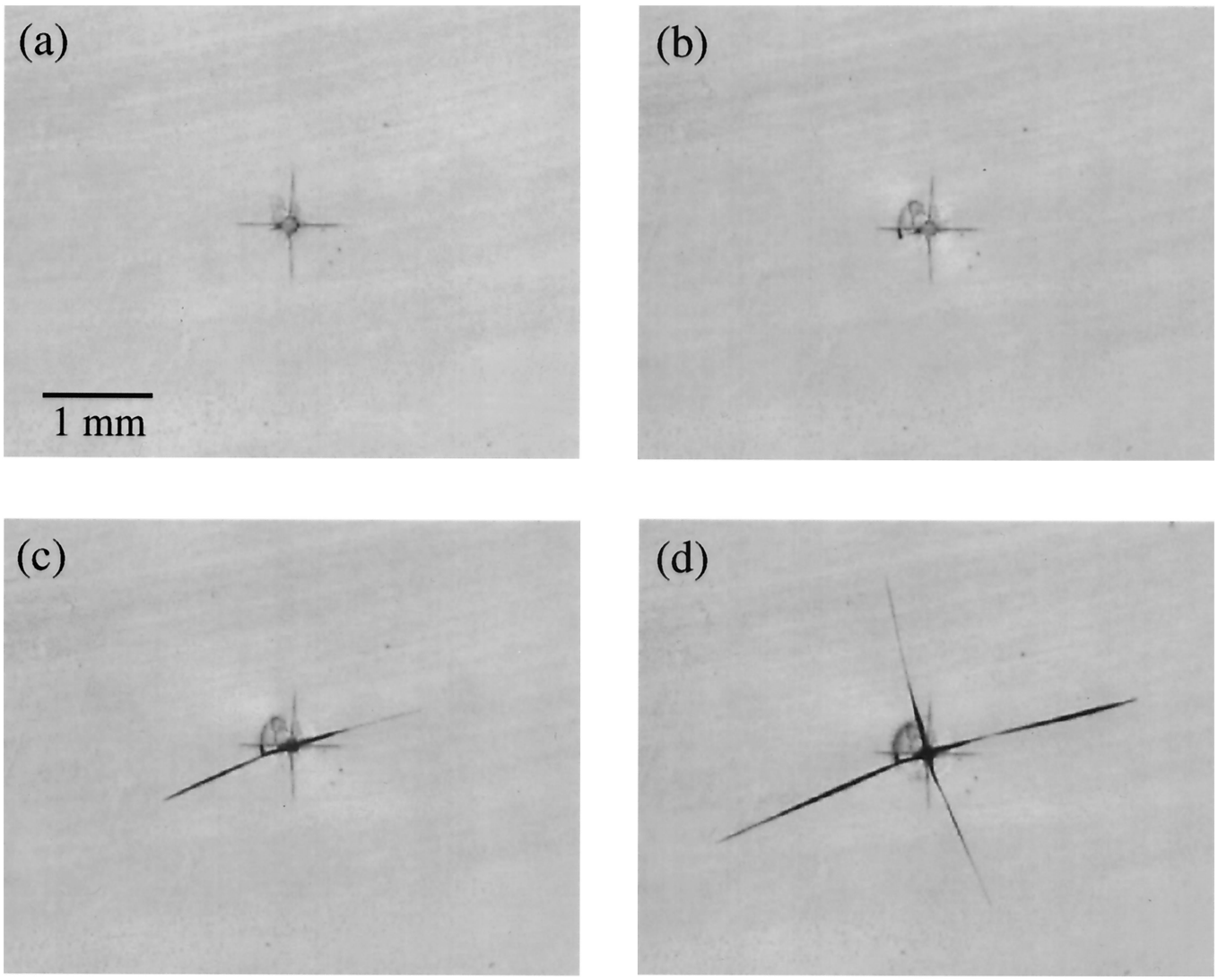

Fig. 5. Micrographs showing *in situ* radial crack growth evolution in glass/polycarbonate bilayers for Vickers load $Q = 100$ N; sphere loads P (a) 0, (b) 70 N, (c) 71 N, and (d) 92 N. Showing immobile original crack, with ultimate pop-in, arrest, and stable extension of entirely new radial crack system from Vickers indentation zone.

The curves in Figs. 6 and 7 are theoretical representations. It might be argued that the anomalous behavior of the bilayer strength data at high Q is entirely attributable to the stress gradient acting on the radial crack (Fig. 2), accountable as the $I(c_*)$ term in Eq. (6). To examine this hypothesis we first adjust the coefficients ψ and χ in Eqs. (6) and (8) (in accordance with $T = 0.67$ MPa·m$^{1/2}$ in Table I) to provide best fits to the monolithic glass flexure data in Figs. 6 and 7. (In these fits, there does appear to be some systematic deviation from classical $Q^{-1/3}$ dependence at higher Q, likely due to stress relaxation from formation of lateral cracks at high loads.[26]) We obtain $\psi = 0.65$ and $\chi = 0.046$ for glass. These values may be compared with previous determinations of the geometry-dependent coefficient $\psi = 0.86$ (from Lawn and Marshall[27]) and 0.77 (from Braun *et al.*[28]) and material-dependent coefficient $\chi = 0.032$ (from Lawn and Marshall[27]) and 0.049 (from Lawn *et al.*[19]) for extending Vickers flaws in monolithic glass flexure specimens. The dashed curves in Figs. 6 and 7 are the regenerated $\sigma_0(c)$ and $\sigma_F(Q)$ functions for the monolith flexure data using these values. Then we use these same coefficients to generate the $\sigma_0(c)$ and $\sigma_F(Q)$ functions for the bilayers—these are the solid curves in Figs. 6 and 7 (note that the solid curve in Fig. 7 does not extend to high Q values, because of the predicted disappearance of an instability branch in this region). The upper axis in Fig. 7 represents the initial radial crack size c_0 prior to strength testing (i.e., $c = c_0$ at $\sigma_0 = 0$ in Eq. (6)). It is apparent in these plots that, even allowing for the scatter in data, the theoretical description is unable to account for the anomalous high strength behavior of the bilayer specimens relative to their monolith flexure counterparts in the large Q region.

To investigate this last point, Fig. 8 compares data for bilayer glass/polycarbonate (B) and as-indented monolith glass biaxial flexure (F) specimens (from Fig. 7) with additional data for monolith specimens covered with a layer of epoxy on an indented surface prior to testing (FE). It is seen that the epoxy coverage does indeed increase the FE strengths, especially at high Q, to somewhere intermediate between the B and F levels. Again, it is as if the epoxy somehow restrains the opening of the original crack walls, increasing the effective toughness of the glass.

(2) Other Ceramic Bilayers

To enable intercomparison between bilayers with different ceramic coating layers, Fig. 9 plots the critical load quantity P_R/d^2 versus Vickers indentation load Q. (The critical loads are divided by the quantity d^2 to reduce the data for coatings of different thicknesses to a common plot, in accordance with Eq. (2)). Error bars indicate standard deviations for a minimum of five tests. The plot includes data for breaks at Vickers indentation sites (filled symbols) and at other (natural flaw) sites (unfilled symbols). Results for unindented specimens are shown as the open boxes at

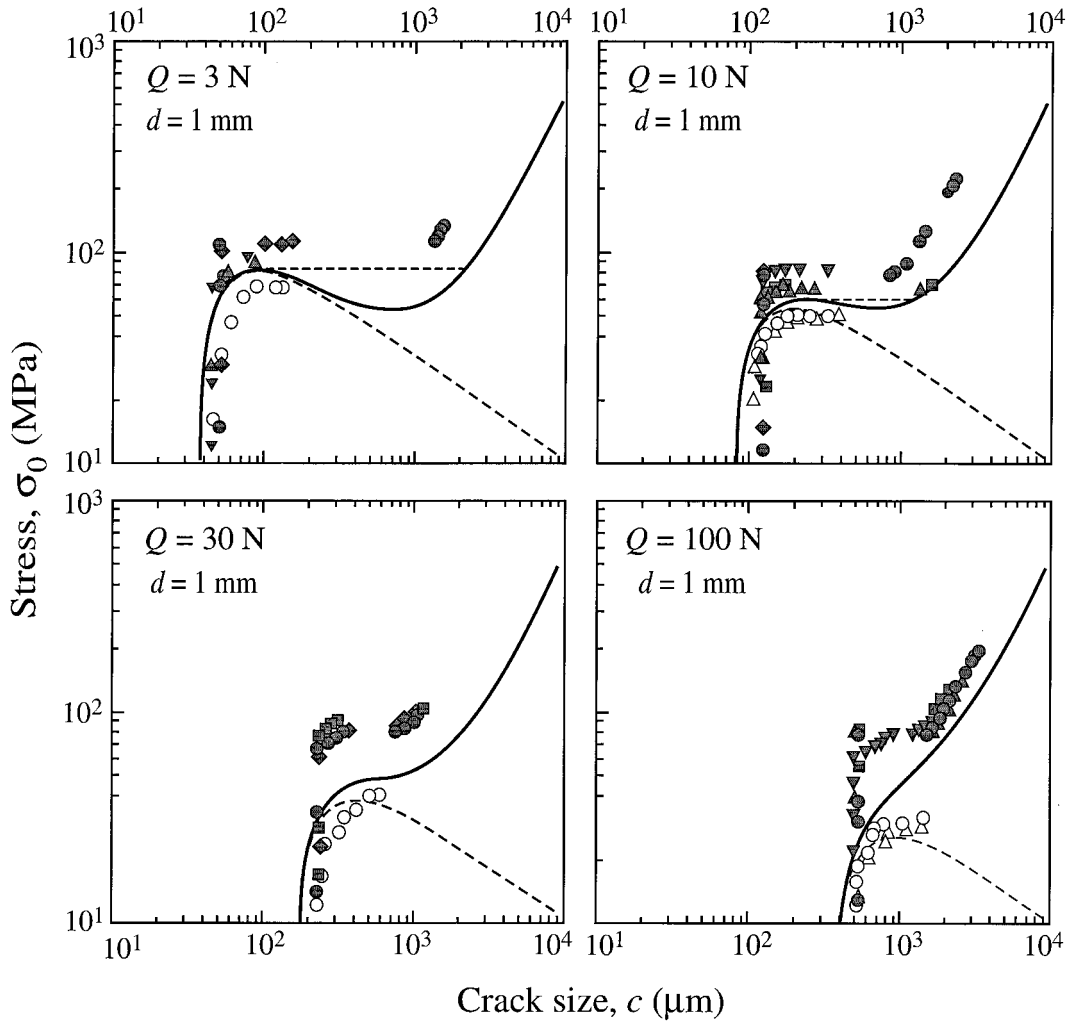

Fig. 6. Growth evolution $\sigma_0(c)$ of Vickers radial cracks in glass/polycarbonate bilayers under contact loading (filled symbols) and glass monolith biaxial flexure specimens (unfilled symbols), glass thickness $d = 1$ mm. Each plot represents a different Vickers load Q, as indicated. Each symbol represents a different Vickers indentation. Dashed curves are best fits to data for monolith flexure specimens in accordance with Eq. (6), and solid curves are the corresponding predictions for bilayers. In all cases, radial cracks initially remain stationary and then undergo stable extension prior to instability at maximum in $\sigma_0(c)$. Cracks in bilayers undergo additional stable extension after pop-in and arrest (horizontal dashed lines)—cracks in monolith specimens proceed to unlimited failure at instability.

the left axis. All materials show a general decline in P_R with increasing Q at given d, confirming the deleterious role of flaw severity, but again with some flattening out at high Q. There are also some interesting material–material distinctions in the data sets. Whereas the critical loads for as-polished surfaces of glass are initially considerably greater than those for porcelain, the reverse is true at high loads Q, commensurate with a lower glass toughness—the porcelain is more flaw tolerant. A similar trend is noted for the alumina relative to the much stronger zirconia—the alumina is less prone to lose its strength.

Figure 10 shows crack extension data for popped-in radials for all ceramic/polycarbonate bilayers. The solid curve is a prediction from the asymptotic Eq. (7), using $\psi = 0.65$ from the above calibration. The results are plotted as $\sigma_0 d^{1/2}/T$ versus $c_* = c/d$ to produce a "universal" diagram. Notwithstanding the considerable crack-to-crack and material-to-material scatter, the data indicate a stabilized growth branch after pop-in and arrest at $c \approx d$, more or less independent of load Q (or initial flaw size c_0).

V. Discussion

We have used controlled Vickers cracks in the undersurfaces of brittle coatings on soft substrates to investigate the role of flaw size in the coating strength properties. Specifically, we have demonstrated that the critical top-surface contact load P_R (or equivalent stress σ_0 at the coating lower surface) to cause the subsurface Vickers-induced radial flaws to undergo unstable growth (pop-in) declines with increasing Vickers indentation load Q (or equivalent initial radial crack size c_0), as expected. Plots such as Figs. 7 and 9 provide a ready, graphic representation of flaw sensitivity of specific coating materials to extraneous lower-surface damage, from either materials preparation or adverse service history—and, as we have seen in the preceding subsection, provide a convenient basis for material evaluation and selection.

Quantitatively, the observed strength degradation for bilayers in Figs. 7 and 9 is not nearly as pronounced as the conventional $Q^{-1/3}$ dependence for monolith flexure specimens. Instead, the bilayer strength data tend to plateau out at high Q (large c_0), indicating substantially enhanced flaw tolerance. Even with due allowance for the considerable tensile stress gradients acting over the radial crack plane, as well as for residual stresses associated with the elastic–plastic Vickers indentation zone, Eq. (6) is unable to account for the anomalous strength behavior. Accordingly, fracture mechanics predictions of coating strengths based on initial flaw size alone will tend to underestimate actual values, more so at larger c_0. At the same time, lower-bound $Q^{-1/3}$ estimates could provide a simple basis for conservative design, with a built-in margin of error.

Further hindering quantitative analysis is the issue of flaw distributions. We have determined strength properties for ceramic coatings containing flaws whose size and location are relatively

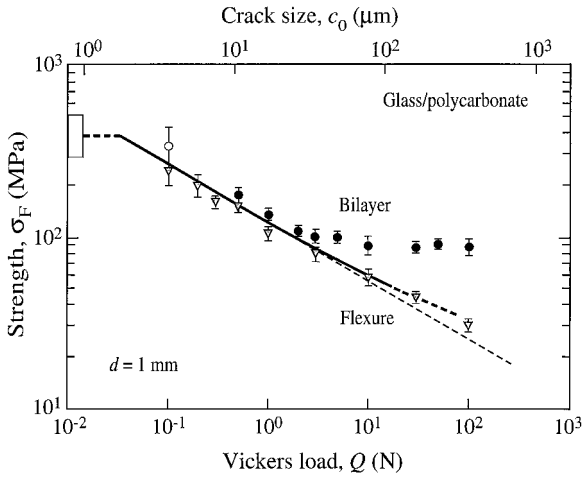

Fig. 7. Strengths $\sigma_F(Q)$ of glass/polycarbonate bilayers, coating thickness d = 1 mm, preindented at the coating undersurfaces with a Vickers indenter at load Q. Data for similarly preindented monolithic flexure specimens included. Filled symbols indicate failures from indentation precracks, unfilled symbols failures from other sites. Dashed curve is best fit of Eq. (8) to the flexure specimen data, solid curve is corresponding prediction for bilayers using Eq. (6). Upper axis is initial radial crack size.

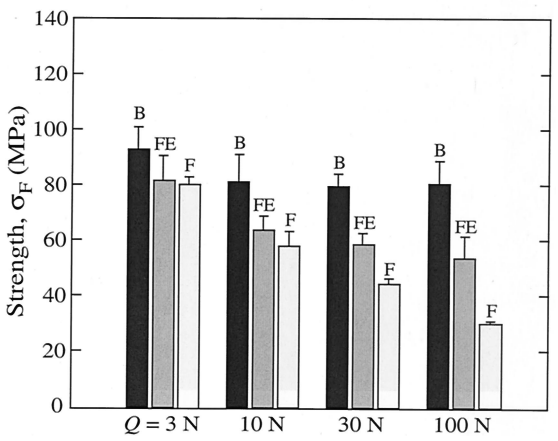

Fig. 8. Strengths σ_F of monolithic glass flexure specimens preindented on the undersurfaces with Vickers diamond pyramid at loads Q. Data compare flexure specimens without (F) and with (FE) layer of epoxy resin applied after indentation. Included are data for epoxy-bonded bilayers (B) from Fig. 7.

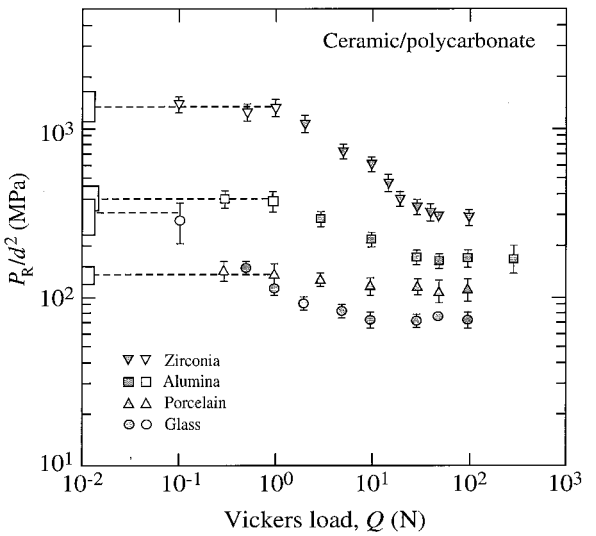

Fig. 9. Reduced critical load quantity P_R/d^2 for instability of radial cracks as function of Vickers load Q for selected ceramic/polycarbonate bilayer specimens. Filled symbols indicate failures from Vickers indentation precracks, unfilled symbols denote failures from other sites, open boxes at left axis failures for unindented specimens. Error bars are standard deviations.

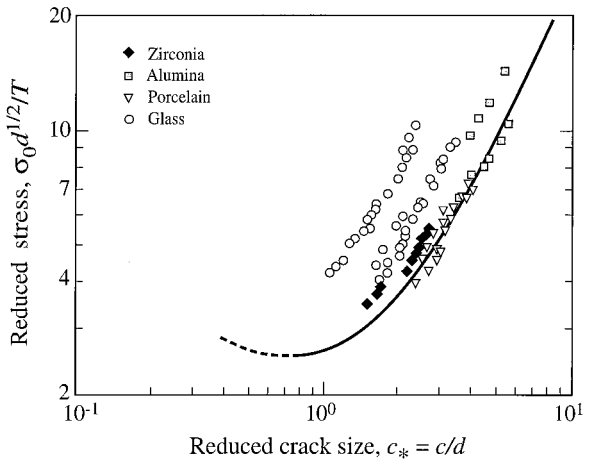

Fig. 10. Plot of normalized stress quantity $\sigma_0 d^{1/2}/T$ as function of normalized crack size $c_* = c/d$ in the second stable growth region, for selected ceramic/polycarbonate bilayer systems. Each symbol represents a different ceramic. Plot shows data for different cracks at different Vickers loads Q (not distinguished). Curve is prediction from Eq. (7).

well controlled. In real coatings the distribution of flaw sizes and locations within the strongly inhomogeneous stress field at the lower surfaces could complicate the strength analysis, increasing the scatter in data still further (especially for thinner coatings with higher stress gradients), necessitating a statistical element.

The simplistic fracture mechanics analysis used here nevertheless appears to account qualitatively for the subsequent second stage of stable extension of popped-in radial cracks after arrest at $c \approx d$ (Fig. 10). This implies that the mechanism responsible for inhibiting the precursor stable growth stage *prior to* pop-in no longer operates *after* pop-in. Even in the second stable region, however, the fracture mechanics should only be considered a crude first approximation, because of limiting assumptions. Most notable of these assumptions are an invariant pennylike crack shape, a constant specimen compliance during the fracture evolution, and a continual equilibrium state—all these conditions are violated to some extent in our tests.

The question remains as to why the strengths for the bilayer specimens are higher than those for corresponding monolithic flexure specimens. We alluded in our discussion of Fig. 8 to a possible role of the epoxy as a restraint on the radial crack opening in initial stressing (Section III (*1*)). It is as if the epoxy somehow enters and "glues" the crack walls together. There is a precedent for such interfacial restraining behavior, from studies of internal corrosion products at cracks in mica and glass after prolonged exposure to moisture.[29] The *in situ* observations in Fig. 5, in which extension occurs from newly initiated rather than existing radial cracks, support this hypothesis. Such effects are more likely to be evident in larger cracks with large crack openings (e.g., as in Fig. 5), consistent with the data trends in Figs. 7 and 9. They are unlikely to persist once the cracks have overcome the wall adhesion and have popped-in,[29] explaining the capacity of the fracture mechanics to account for the second stage of stable growth. If this explanation is valid, we may expect even higher effective strengths for coatings with stronger substrate bonding agents, especially from joining processes at elevated temperatures, as is the case in many brittle coating systems. This is an area that warrants further investigation.

Acknowledgment

The authors thank Herzl Chai for discussions.

References

[1]S. S. Scherrer and W. G. d. Rijk, "The Fracture Resistance of All-Ceramic Crowns on Supporting Structures With Different Elastic Moduli," *Int. J. Prosthodontics*, **6** [5] 462–67 (1993).

[2]S. Wuttiphan, B. R. Lawn, and N. P. Padture, "Crack Suppression in Strongly Bonded Homogeneous/Heterogeneous Laminates: A Study on Glass/Glass-Ceramic Bilayers," *J. Am. Ceram. Soc.*, **79** [3] 634–40 (1996).

[3]L. An, H. M. Chan, N. P. Padture, and B. R. Lawn, "Damage-Resistant Alumina-Based Layer Composites," *J. Mater. Res.*, **11** [1] 204–10 (1996).

[4]H. Liu, B. R. Lawn, and S. M. Hsu, "Hertzian Contact Response of Tailored Silicon Nitride Multilayers," *J. Am. Ceram. Soc.*, **79** [4] 1009–14 (1996).

[5]T. J. Lardner, J. E. Ritter, and G.-Q. Zhu, "Spherical Indentation and Fracture of Glass Plates," *J. Am. Ceram. Soc.*, **80** [7] 1851–62 (1997).

[6]K. S. Lee, S. Wuttiphan, X. Z. Hu, S. K. Lee, and B. R. Lawn, "Contact-Induced Transverse Fractures in Brittle Layers on Soft Substrates: A Study on Silicon Nitride Bilayers," *J. Am. Ceram. Soc.*, **81** [3] 571–80 (1998).

[7]Y. G. Jung, S. Wuttiphan, I. M. Peterson, and B. R. Lawn, "Damage Modes in Dental Layer Structures," *J. Dent. Res.*, **78** [4] 887–97 (1999).

[8]J. R. Kelly, "Clinically Relevant Approach to Failure Testing of All-Ceramic Restorations," *J. Prosthetic Dent.*, **81** [6] 652–61 (1999).

[9]H. Chai, B. R. Lawn, and S. Wuttiphan, "Fracture Modes in Brittle Coatings with Large Interlayer Modulus Mismatch," *J. Mater. Res.*, **14** [9] 3805–17 (1999).

[10]H. Chai and B. R. Lawn, "Role of Adhesive Interlayer in Transverse Fracture of Brittle Layer Structures," *J. Mater. Res.*, **15** [4] 1017–24 (2000).

[11]Y.-W. Rhee, H.-W. Kim, Y. Deng, and B. R. Lawn, "Contact-induced Damage in Ceramic Coatings on Compliant Substrates: Fracture Mechanics and Design," *J. Am. Ceram. Soc.*, **84** [5] 1066–72 (2001).

[12]A. G. Evans, J. W. Hutchinson, and M. Y. He, "Micromechanics Model for the Detachment of Residually Stressed Brittle Films and Coatings," *Acta Mater.*, **47** [5] 1513–22 (1999).

[13]Y.-W. Rhee, H.-W. Kim, Y. Deng, and B. R. Lawn, "Brittle Fracture versus Quasiplasticity in Ceramics: A Simple Predictive Index," *J. Am. Ceram. Soc.*, **84** [3] 561–65 (2001).

[14]P. Miranda, A. Pajares, F. Guiberteau, F. L. Cumbrera, and B. R. Lawn, "Contact Fracture of Brittle Bilayer Coatings on Soft Substrates," *J. Mater. Res.*, **16** [1] 115–26 (2001).

[15]D. B. Marshall, "An Improved Biaxial Flexure Test for Ceramics," *Am. Ceram. Soc. Bull.*, **59** [5] 551–53 (1980).

[16]B. R. Lawn, K. S. Lee, H. Chai, A. Pajares, D. K. Kim, S. Wuttiphan, I. M. Peterson, and X. Hu, "Damage-Resistant Brittle Coatings," *Adv. Eng. Mater.*, **2** [11] 745–48 (2000).

[17]D. B. Marshall and B. R. Lawn, "Residual Stress Effects in Sharp-Contact Cracking: I. Indentation Fracture Mechanics," *J. Mater. Sci.*, **14** [8] 2001–12 (1979).

[18]D. B. Marshall, B. R. Lawn, and P. Chantikul, "Residual Stress Effects in Sharp-Contact Cracking: II. Strength Degradation," *J. Mater. Sci.*, **14** [9] 2225–35 (1979).

[19]B. R. Lawn, A. G. Evans, and D. B. Marshall, "Elastic/Plastic Indentation Damage in Ceramics: The Median/Radial Crack System," *J. Am. Ceram. Soc.*, **63** [9–10] 574–81 (1980).

[20]B. R. Lawn, *Fracture of Brittle Solids*; Chs. 2 and 8. Cambridge University Press, Cambridge, U.K., 1993.

[21]P. Chantikul, G. R. Anstis, B. R. Lawn, and D. B. Marshall, "A Critical Evaluation of Indentation Techniques for Measuring Fracture Toughness: II. Strength Method," *J. Am. Ceram. Soc.*, **64** [9] 539–43 (1981).

[22]B. R. Lawn and M. V. Swain, "Microfracture Beneath Point Indentations in Brittle Solids," *J. Mater. Sci.*, **10** [1] 113–22 (1975).

[23]R. F. Cook, L. M. Braun, and W. R. Cannon, "Trapped Cracks at Indentations: I. Experiments on Yttria–Tetragonal Zirconia Polycrystals," *J. Mater. Sci.*, **29**, 2133–42 (1994).

[24]R. F. Cook and L. M. Braun, "Trapped Cracks at Indentations: II. Fracture Mechanics Model," *J. Mater. Sci.*, **29**, 2192–204 (1994).

[25]J. E. Ritter and M. R. Lin, "Effect of Polymer Coatings on the Strength and Fatigue Behavior of Indented Soda-Lime Glass," *Glass Technol.*, **32** [2] 51–54 (1991).

[26]R. F. Cook and D. H. Roach, "The Effect of Lateral Crack Growth on the Strength of Contact Flaws," *J. Mater. Res.*, **1** [4] 589–99 (1986).

[27]B. R. Lawn and D. B. Marshall, "Residual Stress Effects in Failure from Flaws," *J. Am. Ceram. Soc.*, **62** [1–2] 106–108 (1979).

[28]L. M. Braun, S. J. Bennison, and B. R. Lawn, "Objective Evaluation of Short-Crack Toughness-Curves Using Indentation Flaws: Case Study on Alumina-Based Ceramics," *J. Am. Ceram. Soc.*, **75** [11] 3049–57 (1992).

[29]D. H. Roach, S. Lathabai, and B. R. Lawn, "Interfacial Layers in Brittle Cracks," *J. Am. Ceram. Soc.*, **71** [2] 97–105 (1988). □